Strain-induced elastically controlled magnetic anisotropy switching in epitaxial $La_{0.7}Sr_{0.3}MnO_3$ thin films on $BaTiO_3(001)$

Gyanendra Panchal, D. M. Phase, V. Raghavendra Reddy, and R. J. Choudhary*
UGC DAE Consortium for Scientific Research, University Campus, Khandwa Road, Indore 452001, India

(Received 20 November 2017; revised manuscript received 28 May 2018; published 18 July 2018)

The integration of room-temperature ferromagnetic thin film on ferroelectric substrate with strong magnetoelastic coupling provides a new pathway to tune and improve their functionality for device-application purposes. Epitaxial thin film of ferromagnetic $La_{0.7}Sr_{0.3}MnO_3$ (LSMO) on single-crystalline $BaTiO_3$ (BTO) substrate is observed to be magnetoelastically coupled with BTO substrate with electric-field tunability. The coupling is manifested by discontinuous changes in magnetization as well as in resistivity as BTO undergoes the successive structural phase transitions with temperature. The sign of these abrupt changes shows magnetic-field dependency and is attributed to the in-plane switching of the symmetry of magnetic anisotropy via modification in epitaxial strain-induced distortion as BTO crosses the phase-transition temperature. Under the application of electric field, large magnetization changes are observed via the strain-mediated converse magnetoelectric effect in the LSMO/BTO heterostructure. Up to 55% coercivity change ($\Delta H/H$) and 36% change in squareness (M_r/M_s) of loop are achieved via 8 kV/cm electric field at 210 K. Linear dichroism experiments at the O K edge also show the in-plane orbital anisotropy arising because of the presence of (a, c) stripe domains transferred via pseudomorphic growth on BTO.

DOI: 10.1103/PhysRevB.98.045417

I. INTRODUCTION

Artificial multiferroic (MF) heterostructures consisting of ferromagnetic (FM) and ferroelectric (FE) compounds have attracted great interest over the past few years because these materials are suitable for a wide range of device applications such as magnetic data-storage devices, magnetic- and electric-field sensors, actuators, and microelectromechanical systems [1–3]. Epitaxial thin-film heterostructures are being explored extensively to make magnetoelectric composites because it allows one to maximize the interface strain coupling. In the conventional process, the magnetization of ferromagnetic materials (or polarization of ferroelectric materials) is controlled by means of an applied magnetic field (or electric field) in magnitudes and direction [4]. However, the MF materials are suggested to be more promising candidates for developing and fabricating new electronic storage devices because these materials offer a coupling between two order parameters, such as ferroelectric and magnetic ordering. Recently, electric-field control of magnetization switching or magnetic anisotropy has been shown in many FM/FE multiferroic hybrid structures [5–8]. It is well known that the magnetoelastic effect is transferred via strain across the interface of an FM/FE heterostructure, causing a significant change in the magnetic properties [9]. Among various ferroelectric materials, classical lead-free nontoxic ferroelectric $BaTiO_3$ (BTO) with its unique ferroelectric properties is envisaged as a potential candidate for the practical applications. In bulk form, a typical displacive-type ferroelectric BTO undergoes three successive structural phase transitions: from cubic (C) to tetragonal (T), tetragonal to orthorhombic (O), and orthorhombic to rhombohedral (R) at $T_{C\to T} = 393$ K, $T_{T\to O} = 278$ K, and $T_{O\to R} = 183$ K, respectively. Around these transitions, the lattice constant and spontaneous polarization change abruptly [10,11]. It offers an additional degree of freedom for tuning the strain at the interface of such FM-FE hybrid structure through its first-order structural phase transitions as well as by the electric-field-induced strain through the converse magnetoelectric effect [12]. Such strain-driven reversible and irreversible magnetization switching in the Fe layer was observed in the Fe/BTO heterostructure [13,14]. Similarly, spin reorientation and magnetization switching were also reported for the Fe_3O_4/BTO heterostructure [15,16].

Control of magnetization of the FM/FE heterostructure can be achieved either by structural changes at different temperatures or by application of an electric field on the ferroelectric system, which offers new functionality to many emerging devices for various applications. Among many FM/FE hybrid structures, perovskite manganites/BTO are the well-suited magnetoelastic heterostructures since transport, magnetic, and electronic properties of perovskite manganites are very sensitive to lattice strain and can be easily integrated with BTO due to the similar crystal structure [17–21]. It is known that $La_{0.7}Sr_{0.3}MnO_3$ (LSMO) is a half-metallic hole-doped manganite and has been extensively studied for many fascinating properties such as high-temperature FM to paramagnetic (PM) transition at 350 K, concomitant metal-insulator transition (MIT), colossal magnetoresistance (CMR), etc. [22]. Its integration with BTO is expected to be a potential architect to study the thermal/electric-field-driven strain-induced magnetoelastic effect for the device application. Recently, Preziosi *et al.* showed the nonvolatile modulation of the Mn 3d orbital anisotropy and magnetic moment in LSMO by switching of the

*ram@csr.res.in

ferroelectric polarization [5]. Motti *et al.* showed the subtle interplay between electric-field tunable strain and uniaxial in-plane deformation, which manages the competing FM and antiferromagnetic (AFM) orderings in $La_{0.65}Sr_{0.35}MnO_3$ as probed by x-ray magnetic circular dichroism [23]. It has been shown that magnetization and resistivity behavior reveal abrupt changes across the BTO structural transition temperatures [18]. However, here we explore strain-induced spin reorientation or modulation in magnetic anisotropy in the LSMO/BTO heterostructure. In this study we have prepared room-temperature ferromagnetic LSMO film on single-crystalline BTO substrate and demonstrated the switching of magnetic anisotropy in the epitaxial LSMO/BTO heterostructure. We also study the magnetotransport property of LSMO around the structural phase transition of ferroelectric BTO. The observed anisotropy is shown to be correlated with the electronic structure property of LSMO.

II. EXPERIMENTAL DETAILS

Epitaxial LSMO thin film was grown on BTO (001) substrate by pulsed laser deposition using a KrF excimer laser (248 nm). A single-phase LSMO pallet was used for the deposition. LSMO thin film was deposited at 750 °C substrate temperature with 5 Hz repetition rate in 350 mTorr oxygen partial pressure (OPP) and then cooled in an ambient oxygen environment (500 Torr). During the deposition, the laser energy density at the target surface was kept around 2 J/cm^2 with 4.5 cm target to substrate distance. The nominal thickness of the LSMO film is found to be ∼25 nm. For the structural characterization, the x-ray diffraction measurements were performed using a Bruker D2 PHASER. Reciprocal space mapping (RSM) was performed at room temperature using a Bruker D8-Discover high-resolution x-ray diffractometer (HRXRD). Magnetic measurements were carried out using a 7 Tesla superconducting quantum interference device (SQUID)-vibrating sample magnetometer (SVSM; Quantum Design Inc.). *In situ* electric-field ($\boldsymbol{E}$)-dependent magnetization measurements were carried out by applying an electric field perpendicular to the surface of the film in the same SVSM system. To study the electronic properties of LSMO thin films, x-ray absorption near-edge structure (XANES) spectra at the O K edge in total electron yield (TEY) mode were recorded at room temperature at the polarized light soft x-ray absorption spectroscopy beam line BL-01, Indus-2, RRCAT, India. Electrical-transport and magnetic-transport properties have been performed by the four-probe method using a homemade setup along with an 8 Tesla superconducting magnet (Oxford Instruments, UK). The ferroelectric domains of the $BaTiO_3$ substrate are imaged using a Zeiss polarized microscope in reflection.

III. RESULTS AND DISCUSSION

A. Structural properties

Figure 1(a) corresponds to the room-temperature reciprocal space mapping of bare BTO (T phase) substrate around a symmetric (002) plane in the tetragonal phase. Bragg spots in the substrate point towards the presence of 90° domains, a domains [(200)/(020)], and c domain (002) and whose misorientation is calculated to be $<1°$ [20,17,24]. In Fig. 1(a), the relative intensity of these two domains reveals the presence of the majority of the c domain (002) in the BTO. In a BTO single crystal, in-plane 90° domains (a, c domains) are easily formed with ferroelectric stripe patterns with an elongated c axis rotated by 90° [25,26]. These stripe domains are clearly seen in a polarized microscope image in the T phase of the LSMO/BTO hybrid structure, as shown in the inset of Fig. 1(a). Figures 1(b) and 1(c) show the room-temperature reciprocal maps of 25 nm LSMO film on a BTO substrate around symmetric (002) and asymmetric (–103) planes, respectively. From these scans, the out-of-plane lattice parameter of the a domain of BTO is 3.991 Å and the out-of-plane lattice parameter of the c domain is 4.031 Å. In RSM of an LSMO/BTO (001) heterostructure, we clearly observe the two Bragg spots of the LSMO layer corresponding to bidirectional stripe domain patterns (a domain and c domain) imprinted via underneath ferroelectric BTO. It shows that grown LSMO thin film is epitaxially grown on the ferroelectric stripe domain patterns (90° a/c domains) of BTO substrate. In the reciprocal map around the (002) symmetric plane [Fig. 1(b)], there is no shift in the q_x of the LSMO reflection with respect to the BTO Bragg spot. However, when we see the asymmetric (–103) reflection, we observe the finite shift in q_x of the asymmetric (–103) reflection [Fig. 1(c)] of LSMO with respect to BTO substrate reflection, suggesting that grown LSMO film is partially relaxed. The calculated pseudocubic in-plane lattice parameter of LSMO is 3.88 Å, which is higher than their bulk value 3.869 Å, which is due to substrate-induced in-plane tensile strain leading to the decrease in the out-of-plane lattice parameter to 3.84 Å. Thus, from the RSM, it is revealed that LSMO film is epitaxially grown on BTO substrate and also follows the a, c domains' growth direction in semblance with the a, c domain on the BTO surface due to pseudomorphic growth.

It should be recalled here that the stress in single-crystalline BTO substrate is relieved by the formation of the a-c domain in the form of regular stripe patterns [25]. To further explore these domains, we recorded the optical polarization microscopic images in O and R structural phases of BTO, as shown in Figs. 2(a) and 2(b), respectively. Interestingly, we observe that the width of these stripe domains is completely different in each phase (T, O, and R phase) of BTO and the direction of these stripes is rotated by 45° when the O → R structural phase transition takes place. Here we can see the ferroelectric domain of BTO substrate in the polarized optical image because the thickness of the LSMO layer is less than the penetration depth of the incident light.

B. Magnetic properties

Magnetization versus temperature (M-T) behavior of LSMO thin film deposited on BTO substrate was recorded in field-cooled cooling (FCC) and field-cooled warming (FCW) protocols in the temperature range of 5 to 360 K at 50 Oe magnetic fields. We have performed the measurements with magnetic field applied in the two different directions [010] and [100]. In the FCC cycle, when the magnetic field is applied along the [010] direction [Fig. 3(a)], at temperature 279 K, where the T → O transition of BTO substrate takes place, we

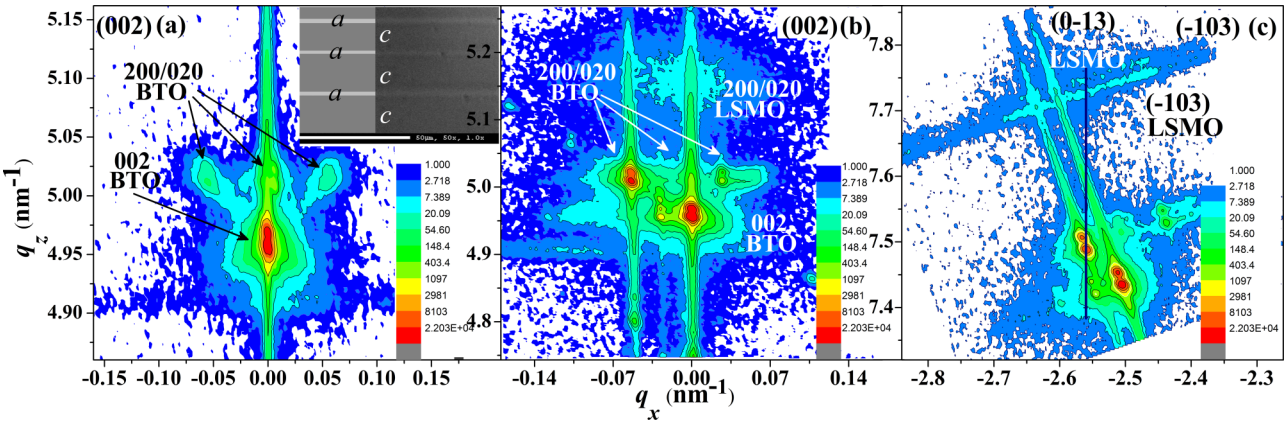

FIG. 1. Reciprocal space maps of (a) bare BTO substrate around symmetric (002) plane and (b) LSMO thin film around symmetric (002) plane. (c) Diffraction spots of LSMO thin film and in-plane 90° a/c domains are shown by arrows. The reciprocal maps around the asymmetric (–103) plane, and diffraction spots of LSMO and BTO, are shown and the relative variation of these spots is highlighted through the vertical lines. The inset in (a) shows the polarization microscopy images of the a-c stripe domains in the T phase (white and gray region).

observe a discontinuous drop by ∼58% in magnetization of the LSMO film. Interestingly, when the temperature reaches to the O → R phase-transition temperature at 186 K, the magnetization jump changes its direction (abrupt increase ∼211%). The value of % jump (increase) or % drop (decrease) is defined by $[(M_f - M_i)/M_i] \times 100$, where M_i and M_f are the magnetization values just before and after the transition, respectively, as marked in Fig. 3(a). When we collect the M-T data in the FCW cycle, we again observe distinct magnetization changes at 194 and 284 K with different magnitude corresponding to the R → O and O → T phase transitions, respectively. The shift in transition temperature in the heating-cooling cycle arises due to thermal hysteresis behavior of the first-order structural phase transition of BTO [10,11]. It should be noted that such abrupt changes in the magnetization are not the characteristics of LSMO; for instance, when LSMO is grown on an $SrTiO_3$ (STO) substrate under a similar condition, M-T does not show any sharp discontinuity, as shown in the inset of Fig. 3(a). This clearly highlights that the magnetic

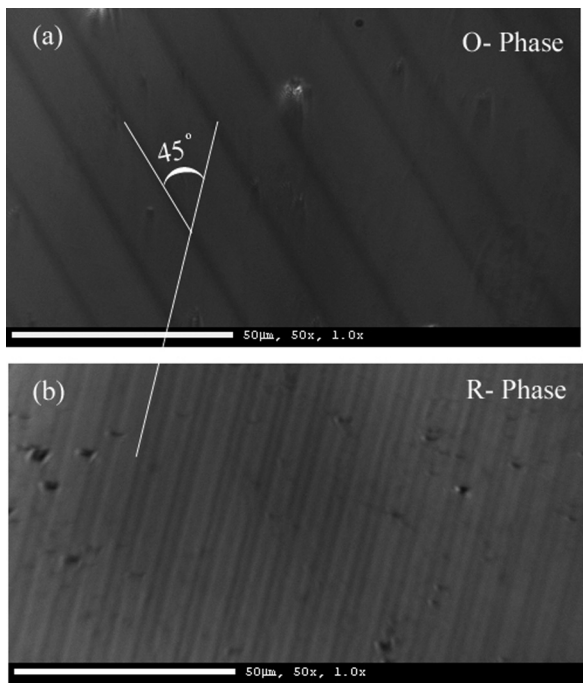

FIG. 2. Polarization microscopy images of the different ferroelectric stripe domain of LSMO/BTO thin film when the BTO substrate is in (a) the orthorhombic (O) phase and (b) the rhombohedral (R) phase.

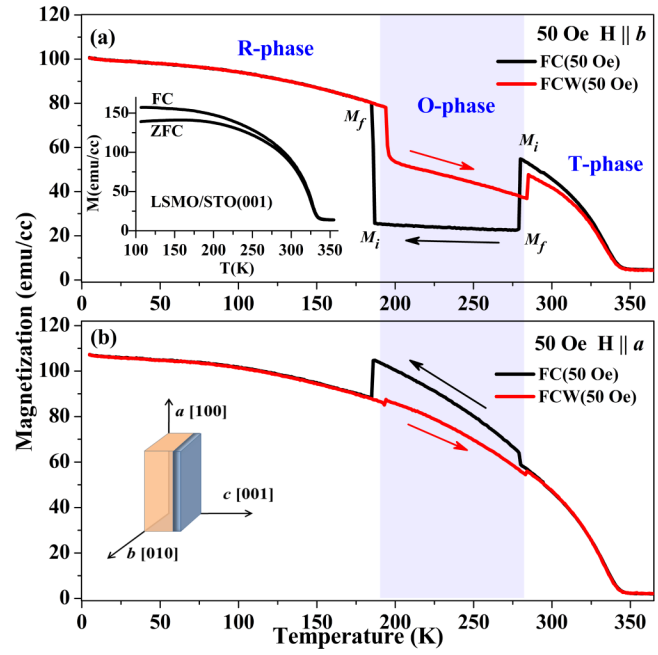

FIG. 3. Magnetization vs temperature (M-T) behavior under 50 Oe field-cooled cooling (black arrow) and field-cooled warming (red arrow) cycles when the applied field is (a) parallel to the b [010] direction and (b) parallel to the a [100] direction. The inset of (a) shows the M-T of the epitaxial LSMO thin film grown on STO (001) measured at 50 Oe.

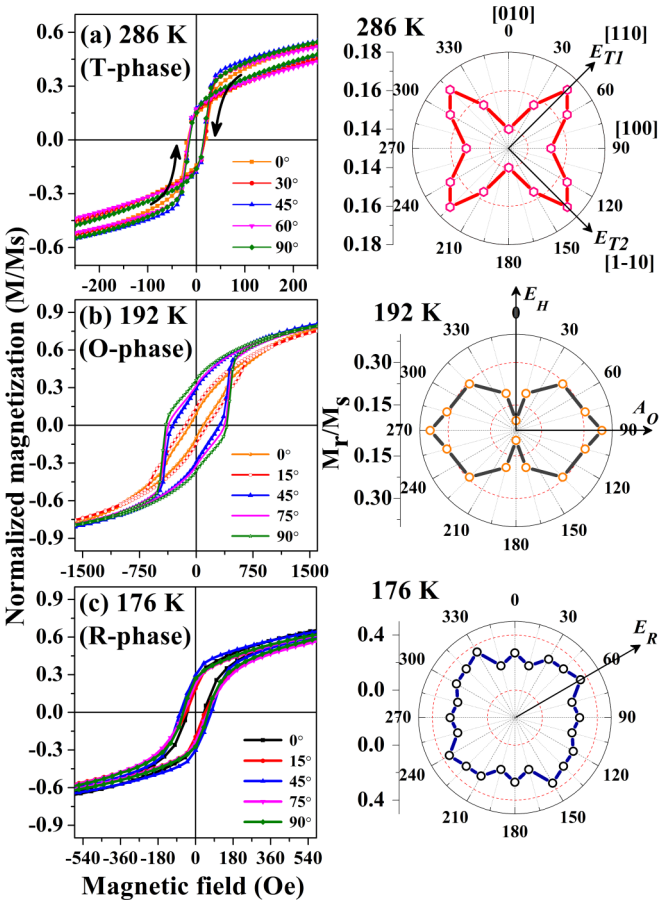

FIG. 4. Normalized magnetization M-H loop at different magnetic-field orientation 0° to 360° at (a) 286 K (T phase), (b) 192 K (O phase), and (c) 176 K (R phase). Angular dependence of normalized remanence magnetization (M_r/M_s) at these temperature values is shown in the form of polar plots.

properties of LSMO are coupled to the BTO structural transition and also mimic the first-order phase transition of the BTO.

Intriguingly, when we applied the same magnetic field along the [100] direction and recorded the data in the FCC cycle [Fig. 3(b)], we observed the distinct jump and drop at 279 and 186 K, respectively, in contrast to the respective drop and jump observed when a magnetic field was applied along the [010] direction. The change in sign of the magnetization jump with changing the applied field direction from the [010] to [100] direction suggests that at the interface, lattice distortion in the LSMO layer induced by the structural phase transition of BTO substrate also affects the in-plane magnetic anisotropy. These observations clearly establish the induced magnetoelastic properties of the LSMO layer due to transfer of the strain via BTO substrate. This strain-induced distortion might be reorienting the magnetization vector from one easy axis to another easy axis [13].

To further explore this switching or reorientation phenomenon, we performed in-plane angle-dependent magnetization versus applied field (M-H) measurements of the LSMO/BTO heterostructure, as shown in Figs. 4(a)–4(c), at different temperature values of 286, 192, and 176 K, corresponding to the T, O, and R phases of BTO, respectively. Subsequently, we shall denote the T, O, and R phases to represent the phase of BTO for the LSMO/BTO heterostructure at that respective temperature. Distinct variation in M-H loop shapes clearly reveals that strain-induced lattice distortion arising due to the successive phase transition of BTO modifies the magnetic anisotropy [27]. These results also clearly indicate that the lattice distortion in the LSMO layer caused due to BTO structural transitions gives rise to a magnetoelastic effect in the LSMO layer. At room temperature, when BTO is in the T phase, we observe an inverse hysteresis loop in a wide in-plane angular range from 0° to 360°, as shown in Fig. 4(a). The decreasing branch [shown by arrow in Fig. 4(a)] cuts the horizontal axis at a positive H value with negative remanence and these features are symmetric for increasing the field branch, which cuts the horizontal axis at negative field with positive remanence akin to inverse hysteresis behavior. These types of unconventional hysteresis loops were observed for $SrRuO_3$-LSMO superlattices and for the NiFe thin film [28,29]. In the case of the LSMO/BTO system, the observed inverse hysteresis is suggestive of the modulation of spin configuration, which arises because of regular stripe patterns of the *a*-*c* domain of the tetragonal phase of BTO coupled with the LSMO film.

Normalized remanence M_r/M_s as a function of the applied magnetic-field orientation in the form of polar plots is displayed in Figs. 4(a)–4(c) in the T, O, and R phases of BTO, respectively. The M_r/M_s plot at 286 K clearly shows the fourfold symmetry in the T phase with two uniaxial magnetic easy axis E_{T1} and E_{T2} around ~45° away from the hard axis [100]. Thus the magnetic easy axis of LSMO in the T phase of BTO orients along the [110] and [1–10] direction of BTO, arising from the epitaxial nature of the film with BTO and the presence of *a*-*c* domains. It should be noted here that the coercivity is not changing with in-plane rotation angle. With decreasing the temperature when the system enters into the O phase, the magnetic anisotropy changes and huge enhancement in coercivity from 20 Oe at 286 K to 400 Oe at 192 K is observed, as shown in Fig. 4(b). The fourfold symmetry behavior of M_r/M_s switches to the twofold symmetry with easy axis A_o along the [100] direction of BTO. When the temperature is further decreased to the R phase, the twofold symmetry of the magnetic anisotropy dramatically disappears and the system becomes almost isotropic [see Fig. 4(c)], owing to the highly symmetric structure of the R phase of BTO [7]. But in Fig. 4(c), small variation in M_r/M_s is observed at 60° so there is a weak anisotropy with an easy axis E_R. The switching of the symmetry of magnetic anisotropy is concomitant with the observed abrupt changes in the magnetization at the transition temperature and further indicates the strain-induced magnetoelastic effect in the LSMO/BTO hybrid structure. Such magnetization switching has prospects in various device applications.

After observing the magnetic switching nature of LSMO film on BTO substrate in the M-H behavior, as discussed above, we now discuss the observation of magnetization switching behavior in M-T. When we record the M-T behavior under 50 Oe applied magnetic field parallel to the [010] direction, the magnetization vector is along easy axis E_{T1} in the T phase. However, when the system enters into the O phase, the

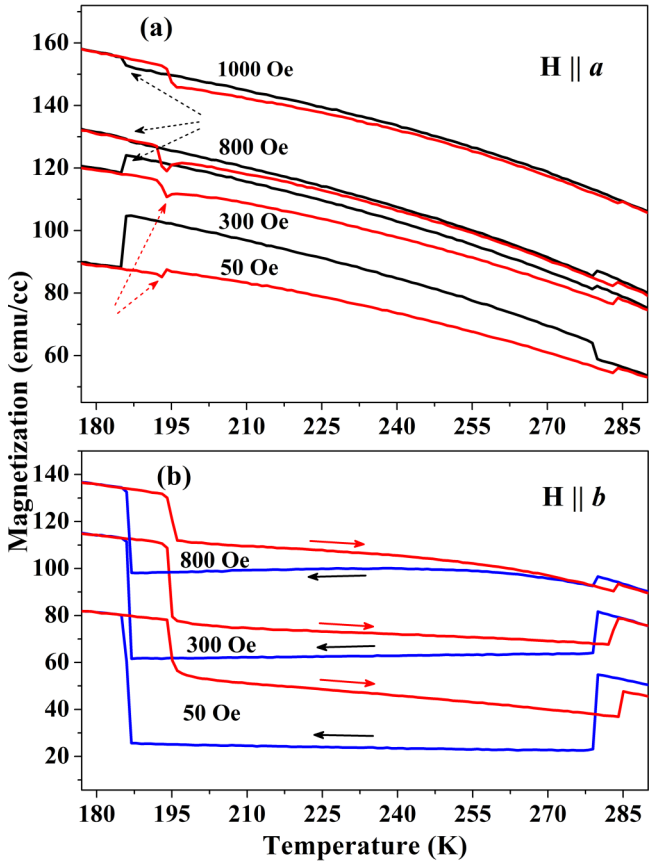

FIG. 5. Magnetization vs temperature (M-T) behavior in FCC and FCW cycles at different applied magnetic field values (a) parallel to the [100] direction and (b) parallel to the [010] direction.

magnetization vector reorients from E_{T1} to another magnetic easy axis A_o, resulting in a drop in magnetization. Upon further cooling, when the system turns in the R phase, the magnetization vector orients along weak easy axis E_R, which is closer to the H direction than A_o [Fig. 4(c)], resulting in a jump in magnetization. More interestingly, it is important to note that the hysteresis loop throughout the O phase shows the combined soft and hard phase like double coercive behavior, which is clearly seen in Fig. 4(b) [30]. Therefore, in the O phase, a fraction of magnetic moments is still trapped along E_H (a hard axis in the O phase), which will require a higher field value to release and align in the direction of the field. However, the measurement is performed at 50 Oe field, which is less than the coercive field ($H_C = 100$ Oe) of the hard magnetic phase. Therefore, when sample enters into the O phase, a drop in magnetization is observed. When we applied 50 Oe along the [100] direction, the magnetization vector is along easy axis E_{T1} in the T phase. When the system enters into the O phase, the magnetization vector reorients from E_{T1} to magnetic easy axis A_o, causing a rise in magnetization. When the system turns in the R phase, the magnetization vector orients along weak easy axis (E_R) of the R phase [Fig. 4(c)], leading to a drop in magnetization.

The FCC and FCW cycles in M-T measurements at different fields applied parallel to the [100] and [010] directions are shown in Figs. 5(a) and 5(b), respectively. In MT behavior, when the magnetic field is applied along the [100] direction, we observed distinct sharp jumps (T → O) and drops (O → R) in the FCC cycle, as we discussed earlier. When the field is increased to 300 Oe, the magnitude of the magnetization drop in the transition O → R decreases and, at higher field value of 800 Oe, these jumps completely disappear. When we record the FCC MT data at 1000 Oe, very interestingly, the distinct discontinuity at the O → R phase transition changed its sign, shown by arrow in Fig. 5(a). In the FCW cycle, this inflection point (the field value at which the magnetization discontinuity changes its sign) in magnetization is observed to occur at the intermediate field between 50–300 Oe, shown by an arrow. Such switching of the sign in the field magnetization direction provides a signature of field-induced modification in the direction of the magnetization vector when the applied field is along the [100] direction. When M-T is recorded at different magnetic field values from 50 to 800 Oe along the [010] direction, there is only a change in the magnitude of the distinct jump around the O → R phase transition of BTO, not the sign.

We mention here that we also performed temperature-dependent magnetic force microscopy (MFM) using the low-temperature MFM from the Autocube system on the thin film of LSMO at different temperature values corresponding to the different phases of the BTO substrate. However, since the magnetic domains are aligned in the film plane, the stray field perpendicular to the film surface is very weak and it is difficult to conclusively detect its distribution on the film surface.

C. Electric-field effect on magnetic properties

So far it is apparent that the magnetic properties of LSMO are strongly modified by the structural phase transition of BTO via magnetoelastic coupling at the interface. It has been shown earlier that under the application of sufficient electric field, most of the ferroelectric domains in BTO are aligned along the field axis and, therefore, BTO transforms from a mixed (*a*,*c*) domain state to a highly populated homogeneous *c* domain configuration. Such modification is known to have implications on the strain-dependent magnetic properties of the magnetic layers grown over the BTO substrate [31,32]. Thus we carried out electric-field-dependent magnetization measurements to look into the effect of electric-field-driven modulation in the magnetization of LSMO film. The *in situ* electric field was applied perpendicular to the LSMO/BTO heterostructure after preparing the gold pads on film and bottom of the substrate (500 μm thick) through copper wires connected by silver paste, as shown by the schematic in Fig. 6(a). M-T behavior under the 50 Oe applied magnetic field along the in-plane [100] direction at different applied electric-field values of 2 and 8 kV/cm are shown in Figs. 6(b) and 6(c). It is observed that at 2 kV/cm electric field, the change in magnetization behavior with respect to the zero electric-field value is very small and visible only in the FCW cycle close to the R-to-O phase transition, as shown in the inset of Fig. 6(b). However, when the electric-field value is increased to 8 kV/cm, the magnetization behavior changes drastically, as shown in Fig. 6(c). It is evident that the magnitude of the jump at 183 K is reduced in the FCC cycle, whereas the sign of jumps in the FCW cycle is completely inverted [see Fig. 6(d)]. Also, at 277 K, the sign

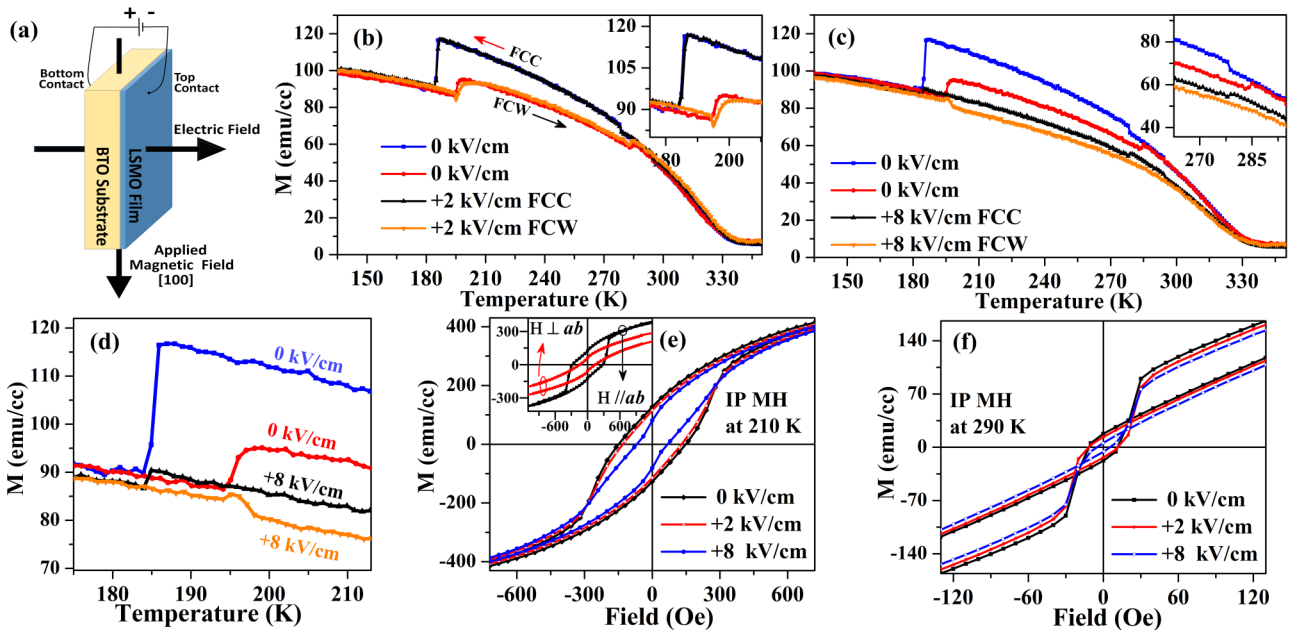

FIG. 6. (a) Schematic of electric-field-dependent magnetization measurements. (b), (c): M-T behavior of a heterostructure without electric field and with electric field of 2 and 8 kV/cm, respectively. The insets in (b) and (c) show the close view of field-induced changes in the magnetization around the R-to-O and O-to-T phase, respectively. (d) A close view of electric-field-dependent M-T around the O-to-R phase transition. In-plane magnetization hysteresis loop with 0, 2, and 8 kV/cm electric field at temperatures (e) 210 K and (f) 290 K. The inset of (e) shows the in-plane and out-of-plane MH at 210 K without application of the electric field.

of the jump in the FCC cycle is changed by application of 8 kV/cm electric field and in the FCW cycle the jump vanishes, as shown in the inset of Fig. 6(c). These findings point towards the change in magnetic anisotropy of LSMO, when an 8 kV/cm electric field is applied across the LSMO/BTO heterostructure.

The modulation in magnetic anisotropy is also reflected from the magnetic hysteresis behavior of LSMO film recorded at different temperature values of 2 and 8 kV/cm electric field, as shown in Figs. 6(e) and 6(f). Figure 6(e) shows the in-plane magnetic hysteresis loop under the different applied electric field 2 and 8 kV/cm perpendicular to the film surface at 210 K. It is evident that with the electric field, coercivity gradually decreases. Overall, up to 55% coercivity change ($\Delta H/H$) and 36% change in squareness (M_r/M_s) of the loop are achieved with 8 kV/cm electric field at 210 K (O phase). The in-plane M-H loop observed at 8 kV/cm is similar to the M-H loop recorded when the magnetic field was along the out-of-plane direction without electric field, as shown in the inset of Fig. 6(e). This indicates that with the electric field, LSMO magnetic moments tend to align along the easy axis direction. Similar changes in the in-plane MH behavior are observed at 290 K (T phase) in the presence of electric field, as shown in Fig. 6(f). Interestingly, the crossover in the loop at a lower magnetic field range tends to merge with decrease in coercivity under the application of electric field. It should be recalled here that in zero electric field, the M-H loop at 290 K was that of an inverse hysteresis behavior and was ascribed to the complex distribution of strain states arising due to stripe domains, which in the electric field is redistributed, with c domains being more populated.

We now discuss the possible reasons behind the observed electric-field-dependent magnetization behavior of LSMO film on BTO substrate. The applied electric field, which is perpendicular to the film surface (i.e., along the c axis of the BTO) leads to elongation of the out-of-plane lattice parameter (c) and contraction of the in-plane lattice parameter (a) of BTO, due to its positive longitudinal (d_{33}) and negative transverse (d_{31}) piezoelectric coefficients, respectively [33]. Therefore, the electric-field-induced contraction in the in-plane lattice parameters of BTO alters the in-plane substrate-induced strain at the interface between LSMO film and BTO substrate, which results in the observed changes in magnetization behavior via magnetoelastic coupling. The magnetoelastic energy giving rise to a uniaxial anisotropy is given by the expression $E_{ME} = \frac{3}{2}\lambda\sigma \sin(2\theta)$, where λ is the magnetostriction constant, σ is the stress, and θ is the angle between the spontaneous magnetization and stress directions [34]. For LSMO, λ is positive [35] and, therefore, $\sigma < 0$ (compressive strain) favors $\theta = \pi/2$ (moment alignment is perpendicular with the stress axis), whereas $\sigma > 0$ (tensile strain) favors $\theta = 0$ (moment alignment is parallel with the stress axis). Without application of the electric field, LSMO film is under the in-plane tensile strain, which leads to in-plane easy axis and out-of-plane hard axis. This is also reflected from the comparison of the out-of-plane and in-plane MH loop recorded at zero electric field at 210 K [inset of Fig. 6(e)], which clearly reveals lower saturation magnetic field for in-plane than out-of-plane MH. It has also been argued earlier that with the application of electric field, the charge-mediated magnetoelectric coupling at the interface of the FM/FE heterostructure would lead to electronic charge modulation (depletion and accumulation at

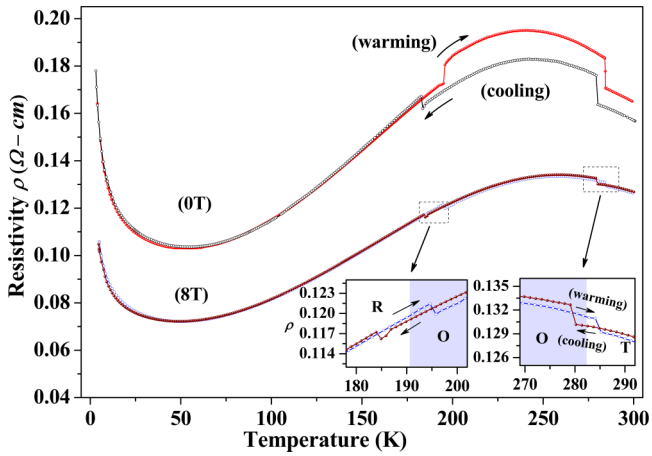

FIG. 7. Temperature dependence of resistivity (ρ) of LSMO/BTO without magnetic field and 8 T applied longitudinal magnetic fields along the in-plane [001] direction. The inset shows the zoomed view of ρ-T behavior in the heating/cooling cycle around the phase transition of BTO.

the interface) via different polarization configuration of the FE layer [8]. Molegraaf *et al.* also reported that in such scenario, the magnetic moment and the Curie temperature are affected [36]. However, in our study, we do not observe any change in saturation magnetization or Curie temperature in magnetization behavior recorded at 0, 2, or 8 kV/cm electric-field values, suggesting that the observed changes arise due to modulation in interface strain between LSMO and BTO causing changes in magnetic anisotropy. The contribution of interface charge carrier density in the present study may not be as dominant as in the studies by Molegraaf *et al.* and Vaz *et al.* due to rather thicker film (25 nm) in the present study than those used in previous studies [8,36].

D. Electrical-transport properties

The electrical resistivity (ρ) versus temperature behavior of heterostructure under the zero and 8 Tesla applied longitudinal magnetic field is shown in Fig. 7. It is observed that LSMO film shows the metal-insulator transition (T_{MI}) at 243 K. This T_{MI} is much lower than the 350 K observed for the bulk LSMO layer. While T_c is comparable to the bulk value, T_{MI} is quite low, possibly due to lower thickness of the LSMO layer (~25 nm), which could be under BTO substrate-induced strain. Interestingly, the sharp jump in resistivity is observed when the BTO substrate crosses the T → O structure phase-transition temperature (280 K). When BTO enters into the R phase at ~183 K, resistivity drops abruptly. At the low-temperature region (below 50 K), the film shows the upturn in resistivity with decrease in the temperature. In the warming cycle also, such discontinuous jump in resistivity appears around the R → O structural phase transition, though with opposite sign of change in resistivity and discontinuous drop around O → T phase transition. Such dependence was also observed in previous reports [18,24]. In the heating cycle, discontinuous jump and drop appear at the slightly higher temperature because of the thermal hysteresis nature of the first-order structural phase transition of BTO. When we performed the ρ versus T measurements under the 8 Tesla magnetic field, the metal-insulator transition shifted towards higher temperature. The distinct jumps and drops around the structural phase-transition temperature of BTO are suppressed in the presence of external field, though not completely. However, the resistivity jump around the R → O phase transition observed in the zero-field ρ-T behavior turned into drop by applying the 8 T magnetic field, as shown in the inset of Fig. 7. These findings further highlighted that the electrical and magnetic properties of the LSMO layer are hugely affected by the underlying BTO substrate via magnetoelectroelastic coupling. We emphasize here that the surface-induced cracking is not an issue because the reversible behavior of resistivity observed in many thermal cycles clearly indicates that it is associated with the intrinsic behavior of the film.

E. X-ray absorption study

To better understand the observed modulation in the magnetic- and electrical-transport properties of LSMO due to BTO-induced strain and its anisotropic nature, we probe its electronic structure using x-ray absorption spectroscopy. It is well known that in 3d transition-metal (TM) oxides, the features in XANES at the O K edge are related to the covalent mixing of metal and oxygen states, and give the information about transition from the oxygen 1s orbitals to unoccupied O 2p-TM 3d hybridized states [37]. As discussed earlier, the LSMO film reveals pseudomorphic growth on BTO substrate and also escorts the *a, c* domains of the underlying substrate. Using a synchrotron source, a linear polarized light can probe the density of the unoccupied state in the direction of electric-field vector ($\boldsymbol{E}$); therefore, linear dichroism (LD) in x-ray absorption spectroscopy (XAS) is an excellent tool to probe the orbital ordering in LSMO epitaxial film [38–40]. Therefore, we have performed room-temperature XAS measurements at the O K edge with linear polarized light in two different configurations: (i) photon polarization vector ($\boldsymbol{E}$) perpendicular to the c direction ($E \perp c$) of the a domain (for the c domain, this configuration will yield $\boldsymbol{E} \| a$) and (ii) $\boldsymbol{E}$ parallel to the c direction ($\boldsymbol{E} \| c$) of the a domain (for the c domain, this configuration will yield $\boldsymbol{E} \| b$). This is performed by rotating the sample in-plane by 90°, as shown in the schematics in Fig. 8(a). The intensity of XAS in these configurations is represented as $I_\perp$ and $I_\parallel$, respectively. The LD is calculated by taking the intensity difference ($I_\perp - I_\parallel$) between the two XAS spectra.

The normalized O K-edge spectra of LSMO/BTO (001) is shown in Fig. 8(b). Experimental schematics used in recording the XANES spectra in the two different orientations are shown in the right section of Fig. 8(a). In the O K-edge spectra, the features A and A' from 529–533 eV are attributed to Mn 3d unoccupied states arising because of the transition from O1s → O2p, which is hybridized with transition-metal Mn 3d orbitals. Bands represented by B and C are attributed to the O 2p overlap with La 5d/Sr 4d and Mn 4sp states, respectively.

In the two different polarization states, the O K edge spectra show major changes in the pre-edge features from 528 to 536 eV. These pre-edge features are primarily related to

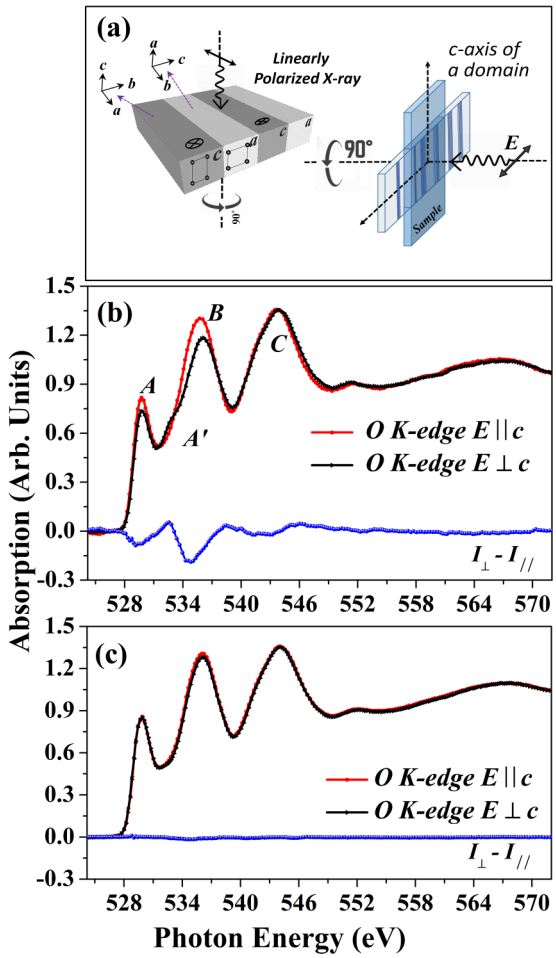

FIG. 8. (a) Schematics of interaction of linear polarized x ray with the different domain of the LSMO layer coupled with the BTO substrate. Room-temperature XAS spectra taken when the photon polarization vector ($\boldsymbol{E}$) is parallel to c and the perpendicular c lattice of the a domain at the O K edge and LD spectra of LSMO film grown on single-crystalline (b) BTO substrate and (c) STO substrate.

strongly hybridized t_{2g} and e_g orbitals of Mn $3d$ with O $2p$ unoccupied states. These features are very sensitive to orbital anisotropy, strain, and lattice distortion [41–45]. In Fig. 8(b), the observed LD shows a negative value in the energy region 528 to 531 eV and positive value close to 532 eV, and is again negative in the energy region 533 to 536 eV. Even though LD at the O K edge cannot directly probe the partial density of states due to hybridization or transition probability issues, it provides a relative information of Mn $3d$ orbitals close to the Fermi level [46]. A thinner sample of LSMO (∼150 u.c.) is also known to reveal LD signal, when two orthogonal polarized lights were used as $E\|c$ and $E\|a$, owing to the octahedral distortion caused by substrate-induced mismatch [47,41]. However, it should be noted here that such film will not reveal LD when XAS is recorded for the $E\|a$ and $E\|b$ configuration. Therefore, to confirm that the observed LD is indeed due to a-c stripe domains in LSMO film on a BTO substrate, we performed similar XANES measurements in the two different photon polarization configurations $E\|c$ and $E\perp c$ at the O K edge on relaxed epitaxial (001) LSMO film (∼300 nm) grown on cubic $SrTiO_3$ (001) substrate, as shown in Fig. 8(c). Such film shows a unidirectional arrangement of unit cells along the c axis and does not have bidirectional a-c-type stripe domains as observed when grown on the BTO (001) substrate. It is evident that such film does not reveal any notable LD. These observations exclude the possibility of any artifacts and confirm that the observed LD signal arises due to the presence of a-c stripe domains.

From these discussions, it is evident that the structural transition of BTO significantly modifies the structural, electrical, magnetic, and electronic properties of LSMO. The clear LD signal at the O K edge reveals the anisotropic nature of hybridization of Mn-$3d$ and O-$2p$ states due to the a-c stripe domains. Such rare coupling along different degree of freedom such as charge, spin, and lattice provides a unique platform to maneuver the electrical and magnetic properties of FM materials such as LSMO using FE domains of BTO through epitaxial interfaces.

IV. CONCLUSIONS

In summary, the epitaxial thin film of LSMO is grown on a single-crystalline ferroelectric BTO substrate by pulsed laser deposition. We have shown that when the BTO substrate undergoes characteristic successive structural phase transitions, strain induced by the lattice distortion leads to discontinuous jumps in the magnetization and resistivity of the LSMO film. Polarization microscopy and RSM measurements clearly demonstrate that a-c domains of BTO are imprinted in the LSMO layer. The large variation in coercivity and sudden switching of symmetry of magnetic anisotropy were observed from fourfold to twofold symmetry followed by twofold to almost isotropic, when BTO passes through T-to-O and O-to-R phase transitions, respectively. The switching of BTO domains along the c axis in the applied electric field alters the in-plane substrate-induced strain at the interface between LSMO film and BTO substrate, which modifies the magnetoelastic anisotropy energy and changes the magnetic easy axis direction from in plane to out of plane. Because of a-c domains in the film, our XLD experiments reveal that the hybridization strength of O $2p$ with Mn $3d$ orbitals is different in the two in-plane directions. The magnetoelastic coupling of ferroelectric domains with ferromagnetic layer and such sharp magnetization anisotropy switching in the manganite-based FM/FE heterostructure via strain-induced distortion have tremendous prospects for application purposes in memory devices.

ACKNOWLEDGMENTS

The authors are thankful to Dr. R. Rawat for providing resistivity measurements and his valuable input. We are also thankful to Dr. A. K. Raychaudhuri for fruitful discussions. The authors also acknowledge Rakesh Kumar Sah for help with the XAS measurements. The authors are thankful to Dr. Manish Kumar for providing the $BaTiO_3$ substrate.

[1] C.-B. Eom and S. Trolier-McKinstry, MRS Bull. **37**, 1007 (2012).
[2] J. F. Scott, Science **315**, 954 (2007).
[3] K. L. Wang, J. G. Alzate, and P. Khalili Amiri, J. Phys. D. Appl. Phys. **46**, 74003 (2013).
[4] C. Song, B. Cui, F. Li, X. Zhou, and F. Pan, Prog. Mater. Sci. **87**, 33 (2017).
[5] D. Preziosi, M. Alexe, D. Hesse, and M. Salluzzo, Phys. Rev. Lett. **115**, 157401 (2015).
[6] E. De Ranieri, A. W. Rushforth, K. Výborný, U. Rana, E. Ahmad, R. P. Campion, C. T. Foxon, B. L. Gallagher, A. C. Irvine, J. Wunderlich, and T. Jungwirth, New J. Phys. **10**, 65003 (2008).
[7] G. Venkataiah, Y. Shirahata, M. Itoh, and T. Taniyama, Appl. Phys. Lett. **99**, 102506 (2011).
[8] C. A. F. Vaz, J. Hoffman, Y. Segal, J. W. Reiner, R. D. Grober, Z. Zhang, C. H. Ahn, and F. J. Walker, Phys. Rev. Lett. **104**, 127202 (2010).
[9] T. Taniyama, J. Phys. Condens. Matter **27**, 504001 (2015).
[10] R. Clarke and IUCr, J. Appl. Crystallogr. **9**, 335 (1976).
[11] H. F. Kay and P. Vousden, London, Edinburgh, Dublin Philos. Mag. J. Sci. **40**, 1019 (1949).
[12] Y. Wang, J. Hu, Y. Lin, and C.-W. Nan, NPG Asia Mater. **2**, 61 (2010).
[13] G. Venkataiah, Y. Shirahata, I. Suzuki, M. Itoh, and T. Taniyama, J. Appl. Phys. **111**, 33921 (2012).
[14] Y. Shirahata, T. Nozaki, G. Venkataiah, H. Taniguchi, M. Itoh, and T. Taniyama, Appl. Phys. Lett. **99**, 2012 (2011).
[15] C. A. F. Vaz, J. Hoffman, A. B. Posadas, and C. H. Ahn, Appl. Phys. Lett. **94**, 111 (2009).
[16] G. E. Sterbinsky, B. W. Wessels, J. W. Kim, E. Karapetrova, P. J. Ryan, and D. J. Keavney, Appl. Phys. Lett. **96**, 1 (2010).
[17] X. Moya, L. E. Hueso, F. Maccherozzi, A. I. Tovstolytkin, D. I. Podyalovskii, C. Ducati, L. C. Phillips, M. Ghidini, O. Hovorka, A. Berger, M. E. Vickers, E. Defay, S. S. Dhesi, and N. D. Mathur, Nat. Mater. **12**, 52 (2012).
[18] M. K. Lee, T. K. Nath, C. B. Eom, M. C. Smoak, and F. Tsui, Appl. Phys. Lett. **77**, 3547 (2000).
[19] W. Wei, J. Chen, K. Zhang, Y. Kou, K. Du, Y. Zhu, W. Wang, X. Li, X. Zhang, X. Gao, L. Zhang, M. Tian, D. Hou, L. Yin, and J. Shen, AIP Adv. **5**, 117135 (2015).
[20] A. Alberca, C. Munuera, J. Tornos, F. J. Mompean, N. Biskup, A. Ruiz, N. M. Nemes, A. de Andres, C. León, J. Santamaría, and M. García-Hernández, Phys. Rev. B **86**, 144416 (2012).
[21] G. Panchal, D. K. Shukla, R. J. Choudhary, V. R. Reddy, and D. M. Phase, J. Appl. Phys. **122**, 85310 (2017).
[22] A.-M. Haghiri-Gosnet and J.-P. Renard, J. Phys. D. Appl. Phys. **36**, R127 (2003).
[23] F. Motti, G. Vinai, A. Petrov, B. A. Davidson, B. Gobaut, A. Filippetti, G. Rossi, G. Panaccione, and P. Torelli, Phys. Rev. B **97**, 094423 (2018).
[24] F. D. Czeschka, S. Geprägs, M. Opel, S. T. B. Goennenwein, and R. Gross, Appl. Phys. Lett. **95**, 14 (2009).
[25] T. H. E. Lahtinen, K. J. A. Franke, and S. van Dijken, Sci. Rep. **2**, 258 (2012).
[26] T. H. E. Lahtinen and S. Van Dijken, Appl. Phys. Lett. **102**, 112406 (2013).
[27] L. Tingxian and L. Kuoshe, J. Appl. Phys. **115**, 44316 (2014).
[28] M. Ziese and I. Vrejoiu, Phys. Status Solidi - Rapid Res. Lett. **7**, 243 (2013).
[29] B. Mora, N. Soriano, C. Redondo, A. Arteche, D. Navas, and R. Morales, Nano Res. **9**, 2347 (2016).
[30] G. Panchal, R. J. Choudhary, and D. M. Phase, J. Magn. Magn. Mater. **448**, 262 (2018).
[31] W. Eerenstein, M. Wiora, J. L. Prieto, J. F. Scott, and N. D. Mathur, Nat. Mater. **6**, 348 (2007).
[32] R. O. Cherifi, V. Ivanovskaya, L. C. Phillips, A. Zobelli, I. C. Infante, E. Jacquet, V. Garcia, S. Fusil, P. R. Briddon, N. Guiblin, A. Mougin, A.A. Ünal, F. Kronast, S. Valencia, B. Dkhil, A. Barthélémy, and M. Bibes, Nat. Mater. **13**, 345 (2014).
[33] R. Tazaki, D. Fu, M. Itoh, M. Daimon, and S. Koshihara, J. Phys. Condens. Matter **21**, 215903 (2009).
[34] S. Sahoo, S. Polisetty, C.-G. Duan, S. S. Jaswal, E. Y. Tsymbal, and C. Binek, Phys. Rev. B **76**, 092108 (2007).
[35] J. M. Vila-Fungueiriño, C. T. Bui, B. Rivas-Murias, E. Winkler, J. Milano, J. Santiso, and F. Rivadulla, J. Phys. D. Appl. Phys. **49**, 315001 (2016).
[36] H. J. A. Molegraaf, J. Hoffman, C. A. F. Vaz, S. Gariglio, D. van der Marel, C. H. Ahn, and J.-M. Triscone, Adv. Mater. **21**, 3470 (2009).
[37] F. M. F. de Groot, M. Grioni, J. C. Fuggle, J. Ghijsen, G. A. Sawatzky, and H. Petersen, Phys. Rev. B **40**, 5715 (1989).
[38] J. Stöhr and H. C. Siegmann, *Magnetism: From Fundamentals to Nanoscale Dynamics* (Springer, New York, 2006).
[39] D. J. Huang, W. B. Wu, G. Y. Guo, H.-J. Lin, T. Y. Hou, C. F. Chang, C. T. Chen, A. Fujimori, T. Kimura, H. B. Huang, A. Tanaka, and T. Jo, Phys. Rev. Lett. **92**, 087202 (2004).
[40] D. Pesquera, M. Scigaj, P. Gargiani, A. Barla, J. Herrero-Martín, E. Pellegrin, S. M. Valvidares, J. Gázquez, M. Varela, N. Dix, J. Fontcuberta, F. Sánchez, and G. Herranz, Phys. Rev. Lett. **113**, 156802 (2014).
[41] D. Pesquera, G. Herranz, A. Barla, E. Pellegrin, F. Bondino, E. Magnano, F. Sánchez, and J. Fontcuberta, Nat. Commun. **3**, 1189 (2012).
[42] M. Abbate, F. M. F. de Groot, J. C. Fuggle, A. Fujimori, O. Strebel, F. Lopez, M. Domke, G. Kaindl, G. A. Sawatzky, M. Takano, Y. Takeda, H. Eisaki, and S. Uchida, Phys. Rev. B **46**, 4511 (1992).
[43] C. Aruta, G. Balestrino, A. Tebano, G. Ghiringhelli, and N. B. Brookes, Europhys. Lett. **80**, 37003 (2007).
[44] B. Wang, L. You, P. Ren, X. Yin, Y. Peng, B. Xia, L. Wang, X. Yu, S.M. Poh, P. Yang, G. Yuan, L. Chen, A. Rusydi, and J. Wang, Nat. Commun. **4**, 2778 (2013).
[45] A. Tebano, C. Aruta, S. Sanna, P.G. Medaglia, G. Balestrino, A.A. Sidorenko, R. De Renzi, G. Ghiringhelli, L. Braicovich, V. Bisogni, and N. B. Brookes, Phys. Rev. Lett. **100**, 137401 (2008).
[46] W. B. Wu, D. J. Huang, G. Y. Guo, H.-J. Lin, T. Y. Hou, C. F. Chang, C. T. Chen, A. Fujimori, T. Kimura, H. B. Huang, A. Tanaka, and T. Jo, J. Electron Spectros. Relat. Phenomena **137**, 641 (2004).
[47] C. Aruta, G. Ghiringhelli, A. Tebano, N. G. Boggio, N. B. Brookes, P. G. Medaglia, and G. Balestrino, Phys. Rev. B **73**, 235121 (2006).